Strong Electron-Deficient Polymers Lead to High Electron Mobility in Air and Their Morphology-Dependent Transport Behaviors

Yu-Qing Zheng, Ting Lei, Jin-Hu Dou, Xin Xia, Jie-Yu Wang, Chen-Jiang Liu, and Jian Pei*

Organic semiconductors are one of the most promising candidates for next-generation electronics applications, such as bio/chemical sensors, flexible displays, logic circuits, and electronic skins.[1–4] The past few years have witnessed momentous changes in the hole mobility of organic semiconductors with a number of p-type organic semiconductors surpassing the benchmark mobility of 10 cm^2 V^{-1} s^{-1}.[5] Hole mobilities are over 40 cm^2 V^{-1} s^{-1} for small-molecule single-crystal and thin-film field-effect transistors (FETs),[6,7] 12 cm^2 V^{-1} s^{-1} for polymer FETs,[8] and 36.3 cm^2 V^{-1} s^{-1} for unidirectional aligned polymer FETs.[9] In sharp contrast, the state-of-art electron mobilities are 12.6 cm^2 V^{-1} s^{-1} for single-crystal FETs,[10] 3.5 cm^2 V^{-1} s^{-1} for small-molecule thin-film FETs,[11] 7.0 cm^2 V^{-1} s^{-1} for polymer FETs in inert atmosphere,[12] and only 1.7 cm^2 V^{-1} s^{-1} for polymer FETs operated under ambient conditions.[13] These values are almost one order of magnitude lower than those of their p-type counterparts. To achieve great circuit speeds, low power dissipation, and high noise immunity in organic complementary circuits, both p- and n-type transistors with congruent performance are desired.[14,15] However, the imbalanced development of organic semiconductors has been limiting the broad applications of organic electronics that require both high-performance p-type and n-type organic semiconductors ever since the discovery of organic semiconductors.[16–18]

Recently, many reported high-mobility conjugated polymers, such as benzothiadiazole (BT),[9,19–21] diketopyrrolopyrrole (DPP),[22–27] isoindigo (II)[28–30] based polymers, represent obvious nonlinear transfer curves with higher mobility in the low gate voltage (V_G) region. However, the mechanism is still under debate.[31,32] Nguyen and co-workers proposed that for p-type polymers, electron trapping and the subsequently formed —SiO^- charges contribute to the nonlinear transfer curves. When the dielectric layer was changed to defect-free BCB (a polymer dielectric formed by divinyl-tetramethyl-siloxane-bis(benzocyclobutene) derivative), the mobility of polymer was no longer gate dependent. Nevertheless, this mechanism cannot explain the nonlinear transfer characteristics of conjugated polymers with defect-free polymer dielectrics and also cannot explain those of n-type or ambipolar polymers.

Here we report a new polymer building block F_4BDOPV, which displays a deep LUMO level down to −4.44 eV, representing the most electron-deficient building block ever reported.[33] On the basis of F_4BDOPV, two copolymers F_4BDOPV-2T and F_4BDOPV-2Se were prepared through Stille polymerization. High apparent electron mobilities of up to 14.9 cm^2 V^{-1} s^{-1} were extracted from F_4BDOPV-2T FET devices measured in air, several times higher than the hitherto best n-type conjugated polymers.[13] The polymers showed problematic nonlinear transfer characteristics. We found that these nonlinear transfer curves are highly correlated with the film preparation method, which can be attributed to their different microstructures.

To realize air-stable electron transport and avoid the electrochemical oxidation by H_2O and O_2, a low LUMO energy level below −4.9 eV is required.[34] Organic materials with such large electron affinities are very rare, but recent studies show that materials with LUMO levels at around −4.1 to −4.3 eV may exhibit air-stable electron transport due to an overpotential of oxygen reduction.[35–37] However, most of the polymer building blocks have LUMO levels higher than −4.0 eV (**Figure 1**a), unstable for efficient electron transport.[33,38] Recently, we developed an electron-deficient building block, namely benzodifurandione-based oligo(p-phenylene vinylene) (BDOPV),[39] which shows a LUMO level of −4.24 eV. After polymerization with 2,2′-bithiophene, BDOPV-2T exhibited a LUMO level of −4.15 eV, which is a little bit higher for air-stable n-type OFET devices and therefore BDOPV-2T showed ambipolar transport properties in air.[40] Thus, four fluorine atoms are introduced to BDOPV giving F_4BDOPV further lowered LUMO level (Figure 1b). 2,2′-Bithiophene and 2,2′-biselenophene are used as the donor units to construct conjugated polymers F_4BDOPV-2T and F_4BDOPV-2Se (see Scheme S1, Supporting Information). We calculated the energy levels of the building blocks (Figure 1a) and the corresponding polymers with bithiophene as donor unit by extrapolating from the values computed for the oligomers (Figure S1, Supporting Information). F_4BDOPV

Y.-Q. Zheng, Dr. T. Lei, J.-H. Dou, Prof. J.-Y. Wang, Prof. J. Pei
Beijing National Laboratory for Molecular Sciences (BNLMS)
Key Laboratory of Bioorganic Chemistry and Molecular Engineering of Ministry of Education
Center of Soft Matter Science and Engineering
Key Laboratory of Polymer Chemistry & Physics of Ministry of Education
College of Chemistry and Molecular Engineering
Peking University
Beijing 100871, China
E-mail: jianpei@pku.edu.cn
X. Xia, Prof. C.-J. Liu
Physics and Chemistry Detecting Center
Key Laboratory of Oil & Gas Fine Chemicals of Ministry of Education
School of Chemistry and Chemical Engineering
Xinjiang University
Urumqi 830046, China

COMMUNICATION
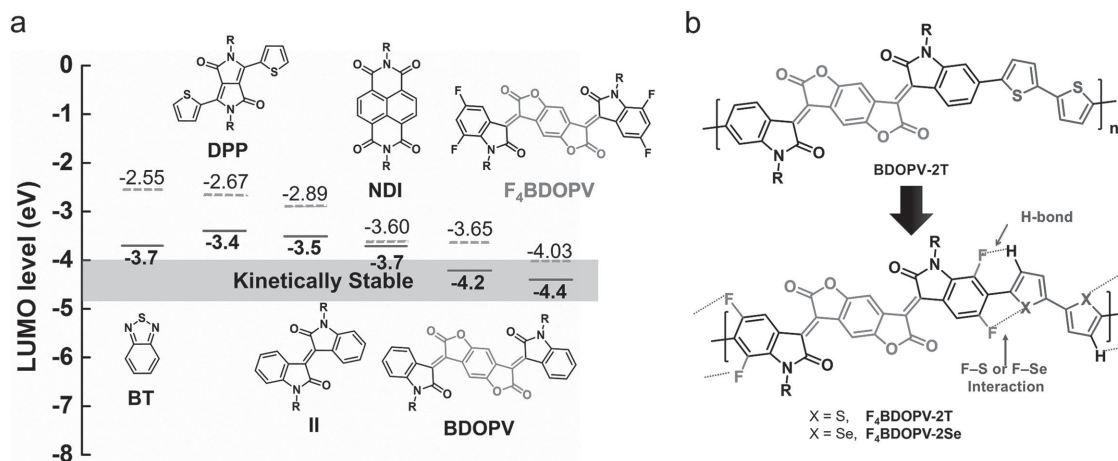
Figure 1. a) Molecular structures and calculated (dotted lines) and measured (solid lines) LUMO levels of electron-deficient building blocks used for polymer FETs. The calculated levels are systematically 0.2–0.4 eV higher than measured ones, which is often observed in literatures using B3LYP as functional.[58,59] Both calculated and measured data show that F$_4$BDOPV unit exhibits the lowest LUMO level ever reported for polymer building blocks, which may lead to kinetically stable electron transport for polymers. b) Design strategy of F$_4$BDOPV-based polymers.

monomer represents the lowest LUMO level (−4.44 eV) among these polymer building blocks. Theoretical calculations showed that the introduction of fluorine atoms obviously lowered the LUMO levels of F$_4$BDOPV-2T and F$_4$BDOPV-2Se by about 0.3 eV as compared with that of BDOPV-2T (Figure S1, Supporting Information). Although fluorine atom has a van der Waals radius of 1.47 Å, larger than that of hydrogen (1.20 Å),[41] the introduction of fluorine atoms does not increase the phenyl-thienyl dihedral angle (**Figure** 2b). Instead, the dihedral angle between acceptor part and flanked thiophene decreases from 21.9° in BDOPV-2T to 9.6° in F$_4$BDOPV-2T, and the F—H (2.27 Å) and F—S (2.70 Å) distances in F$_4$BDOPV-2T are considerably shorter than the sum of F—H (2.67 Å) and the sum of F—S (3.20 Å) van der Waals radii, respectively.[41] The relaxed potential energy scan of dihedral angle between F$_4$BDOPV and flanked thiophene showed that F$_4$BDOPV-2T has a large rotational barrier of 3.8 kcal mol^{-1} between two planar conformations (Figure S3, Supporting Information). These results indicate that fluorine substitution can planarize the polymer

backbones and lock their conformation through the non-covalent bonding interactions of F—H and F—S. Locked conformation can result in rigid polymer backbones with less torsional disorders along polymer backbones, thereby leading to better π-π stacking, higher film crystallinity and improved charge transport.[42–44]

Both polymers show similar profiles with dual-band absorption (Figure 2a and S8a, Supporting Information). The bandgaps calculated from the onset of the absorption profiles are close for both polymers, 1.31 eV for F$_4$BDOPV-2T and 1.29 eV for F$_4$BDOPV-2Se. It is known that intermolecular interactions and conformational changes in conjugated polymers can shift the absorption spectrum and change vibrational peak intensity.[45] Compared with those in solution, absorption spectra of both polymers in thin films only show negligible red-shift (Figures S6 and S8a, Supporting Information), suggesting that both polymers might form some preaggregates in solution due to the strong interchain interactions.[46] A noticeable increase of 0–0 vibrational peak was observed from solution to film
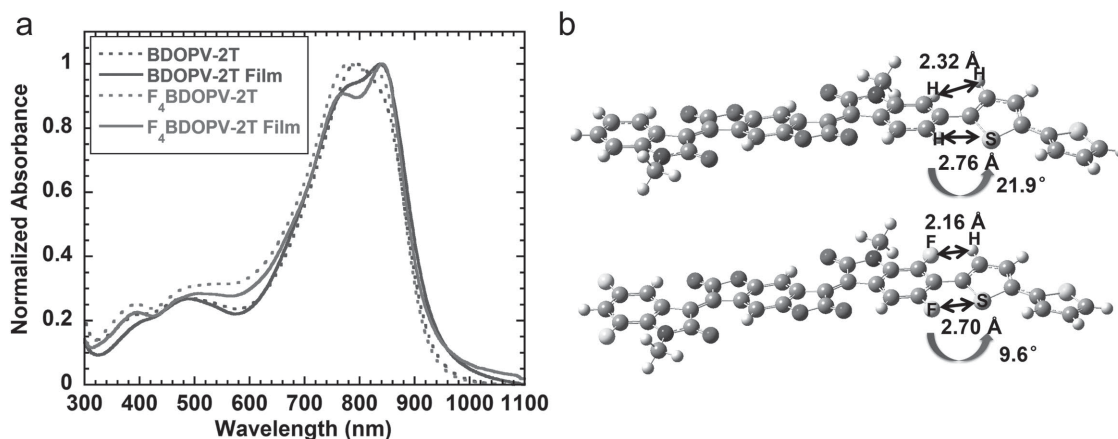
Figure 2. a) Normalized absorption spectra of BDOPV-2T and F$_4$BDOPV-2T in CHCl$_3$ (10^{-5} M) and in thin films. b) Molecular models of BDOPV-2T (above) and F$_4$BDOPV-2T (below) fragments (calculated with B3LYP/6-311G(d,p)). F$_4$BDOPV showed more planar backbone than BDOPV-2T due to the nonbonding interactions.

Table 1. Optical and electrochemical properties of BDOPV-2T, F$_4$BDOPV-2T and F$_4$BDOPV-2Se.

Compounds	λ_{max}^{sol} [nm][a]	λ_{max}^{film} [nm]	E_g^{Opt} [eV][b]	E_{LUMO}^{CV} [eV][c]	E_{HOMO}^{CV} [eV][c]	E_{LUMO}^{PES} [eV][d]	E_{HOMO}^{PES} [eV][e]
BDOPV-2T	794	834	1.31	−4.15	−5.72	−4.35	−5.66
F$_4$BDOPV-2T	838	844	1.31	−4.32	−5.96	−4.54	−5.85
F$_4$BDOPV-2Se	850	862	1.29	−4.34	−5.91	−4.54	−5.83

[a]10^{-5} M in chloroform; [b]Estimated from the onset of the absorption spectra of thin films; [c]Cyclic voltammetry determined with Fc/Fc$^+$ (E_{HOMO} = −4.80 eV) as external reference; [d]Determined by PES and optical bandgap, E_{LUMO}^{PES} = E_{HOMO}^{PES} + E_g^{Opt} ; [e]Determined by PES.

state, indicating a further planarization of polymer backbone in solid state. Compared with BDOPV-2T, the introduction of four fluorine atoms provides F$_4$BDOPV-2T with increased 0–0 and decreased 0–1 peak intensities in both dilute solution and thin film, suggesting that F$_4$BDOPV-2T may adopt a more planar backbone conformation, which is in good agreement with the molecular modeling results. After the introduction of fluorine atoms, the LUMO energy level of F$_4$BDOPV is noticeably lowered by 0.2 eV, down to −4.44 eV (see cyclic voltammogram, Figure S7, Supporting Information). The LUMO level of F$_4$BDOPV-2T reaches −4.32 eV, 0.17 eV lower than that of BDOPV-2T. With 2,2′-biselenophene as the donor, F$_4$BDOPV-2Se shows a smaller bandgap of 1.29 eV with a LUMO level

of −4.34 eV and a HOMO level of −5.91 eV (Figure S8b, Supporting Information and **Table 1**). The CV results agreed well with the energy levels calculated from photoelectron spectroscopy (PES) and optical bandgaps, which gives HOMO/LUMO levels of −5.85/−4.54 eV for F$_4$BDOPV-2T and −5.83/−4.54 eV for F$_4$BDOPV-2Se (Figure S9, Supporting Information and Table 1). To our knowledge, these polymers are the most electron-deficient conjugated polymers reported to date.[16]

Top-gate/bottom-contact (TGBC) FET devices with CYTOP (≈500 nm) as the dielectric layer were fabricated. Compared with the ambipolar polymer BDOPV-2T,[40] F$_4$BDOPV-2T showed typical n-type transport characteristics in air (**Figure 3**b,c). Several annealing temperatures were tried and
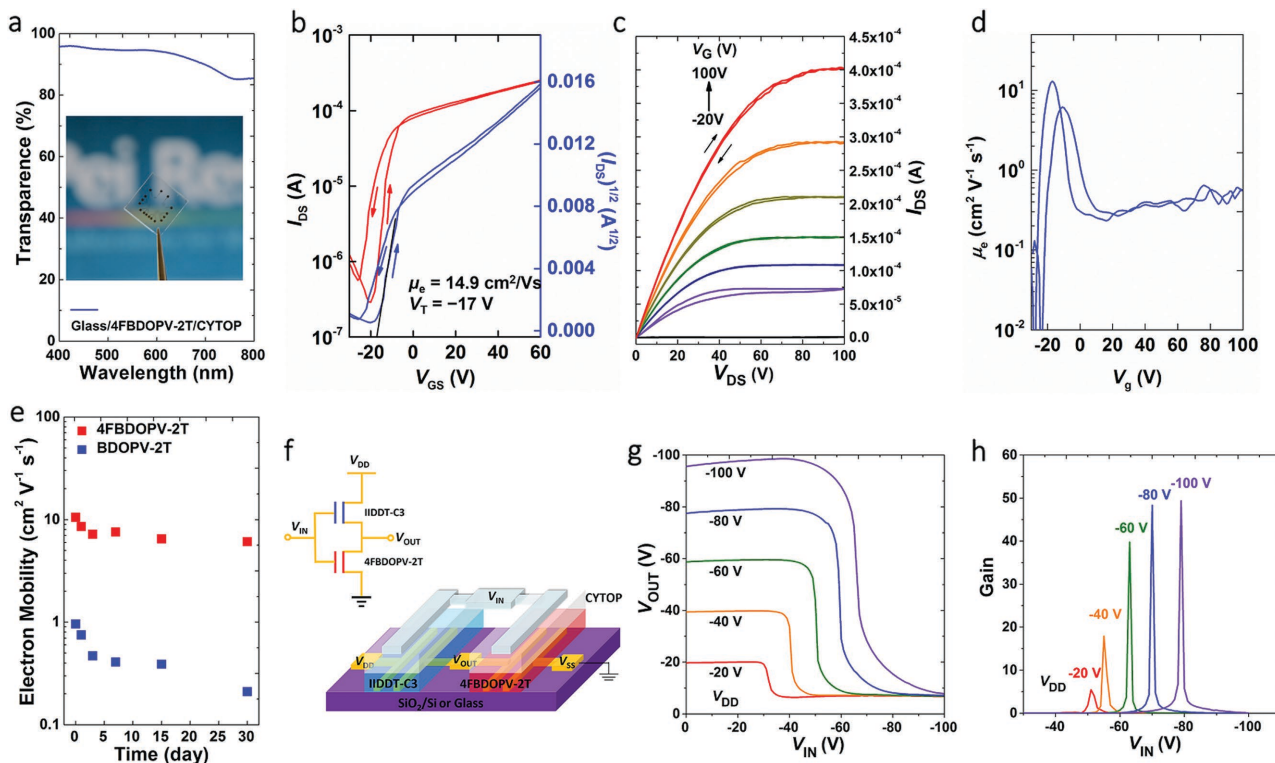
Figure 3. a) Transmission spectrum of the glass/F$_4$BDOPV-2T/CYTOP device. Inset: photograph of a F$_4$BDOPV-2T device with glass substrate. b) Transfer and c) output characteristics (V_{DS} = 100 V) for F$_4$BDOPV-2T based FET devices annealed at 160 °C (L = 100 μm, W = 2000 μm, C$_i$ = 3.7 nF cm^{-2}). The electron mobility of 14.9 cm^2 V^{-1} s^{-1} in the saturation regime was calculated from the slope obtained by linear fitting of (I$_{DS}$)$^{1/2}$ and V_G in the range from −16 to −6 V. d) Mobilities as a function of gate voltage. The mobility is calculated from the local slope of the square root of the transfer curve at saturation regime (I$_{DS}^{1/2}$ versus V_G). e) Stability comparison of the F$_4$BDOPV-2T and BDOPV-2T devices in air (R$_H$ = 50%–60%). f) Electrical connections and schematic device configuration of an inverter. The inverter device consists connected p-type (IIDDT-C3) and n-type (F$_4$BDOPV-2T) TFT devices. g) Static switching characteristics of an inverter tested in air. The complementary inverter displayed clearly on and off states with the V_{OUT} voltages close to the V_{DD} supply voltage. h) Gains of an inverter at different voltages. A high gain value of up to 50 was demonstrated, indicating a fast and low-power-consumption switching property.

COMMUNICATION

Table 2. Summary of OFET performance and GIXD results of the polymers.

Polymer	μ [cm^{2}V^{-1}s^{-1}][a] (low V_G region)	μ [cm^{2}V^{-1}s^{-1}][b] (high V_G region)	μ [cm^{2}V^{-1}s^{-1}][c] (linear curve)	V_T[d] [V]	I_{on}/I_{off}	d [Å][e]		Coherence length [nm]
						L	π	
F$_4$BDOPV-2T[f] (500 rpm)	14.9 (9.0)	1.24 (0.68)	/	−17	/	10^3–10^4	28.4	3.52	15.5
F4BDOPV-2T[g] (2000 rpm)	7.7 (2.63)	0.76 (0.63)	1.56 (1.01)	−20	+3	10^3–10^4	28.4	3.52	6.78
F$_4$BDOPV-2Se	6.14 (3.20)	0.64 (0.32)	/	+3	/	10^3–10^4	28.6	3.55	7.30

[a]Devices were measured under ambient conditions (R_H = 50%–60%). Maximum values (average values). Mobility extracted from the low V_G region of nonlinear transfer curves; [b]Mobility extracted from the high V_G region of nonlinear transfer curves; [c]Mobility extracted from the near-ideal transfer curves; [d]The threshold voltages shown here belong to the device with the highest electron mobility of both polymers; [e]Lamellar (L) and π–π stacking (π) distances determined by GIXD experiments; [f]Thin films fabricated using spin-coating speed of 500 rpm; [g]Thin films fabricated using spin-coating speed of 2000 rpm.

annealing at 160 °C gave the best device performance (Tables S2 and S3, Supporting Information). F$_4$BDOPV-2T showed the highest electron mobility of 14.9 cm^2 V^{-1} s^{-1} and an average mobility of 9.0 cm^2 V^{-1} s^{-1} with on/off ratios of 10^3 to 10^4 (**Table 2**). We noticed that the transfer curve of F$_4$BDOPV-2T shows nonlinear behavior (Figure 3d). The mobilities extracted from low V_G region of F$_4$BDOPV-2T devices fabricated with a low spin-coating speed of 500 rpm are in the range from 3.72 to 14.9 cm^2 V^{-1} s^{-1}, while the mobilities in the high V_G region has the highest value of 1.24 cm^2 V^{-1} s^{-1} and an average value of 0.68 cm^2 V^{-1} s^{-1}. The output curves show good saturation in the low V_G region, therefore the devices are operated at saturation regime ($V_D > V_G - V_T$) when V_D = 100 V. Thus, the standard formula is valid. Since the transfer curve is not ideal, such high mobility may not reflect the intrinsic charge transport properties of the polymer. After all, we still consider this performance a huge improvement compared with other n-type organic semiconductors. The transfer and output characteristics show very small hysteresis, suggesting that only a few traps exist even under oxygen exposure. No obvious injection barrier is observed in the output curves, indicating a good ohmic contact between the polymer and electrode. After replacing thiophene with selenophene, F$_4$BDOPV-2Se also showed impressive n-type performance with the highest electron mobilities of up to 6.14 cm^2 V^{-1} s^{-1} and an average mobility of 3.20 cm^2 V^{-1} s^{-1} in the low V_G region, while the highest mobilities in the high V_G region is 0.64 cm^2 V^{-1} s^{-1} and an average value of 0.32 cm^2 V^{-1} s^{-1} (Figure S10, Supporting Information and Table 2). The threshold voltages of both polymers are in the range from −30 to 5 V. The variation of threshold voltage is a common phenomenon for organic semiconductors.[11,47] We hypothesize that the variation of threshold voltage may be due to the status of interface between dielectric layer and polymer layer.

The stability of F$_4$BDOPV-2T and BDOPV-2T devices were compared by storing the devices in air (R_H = 50%–60%) (Figure 3e). After 30 d, benefited from the low LUMO levels, the electron mobility of F$_4$BDOPV-2T device decreased from 10.6 to 6.1 cm^2 V^{-1} s^{-1}, only 40% decrease from the original mobility, whereas the electron mobility of BDOPV-2T decreased significantly from 0.96 to 0.21 cm^2 V^{-1} s^{-1}. The good air stability of F$_4$BDOPV-2T can be attributed into two features: (1) the strong electron-deficient building block F$_4$BDOPV endows the polymer with a low-lying LUMO level; (2) the planar/rigid backbone and strong interchain interactions provide the polymer with highly ordered molecular packing and small π–π stacking distance, which can increase the oxygen penetration

barrier.[37,48] Both features together contributed to the good device stability and high electron mobility of F$_4$BDOPV-2T.

A voltage inverter is the basic element for logical functions (such as NAND and NOR) and ring oscillators.[49] To realize low power dissipation and high noise immunity inverters, both p-type and n-type semiconductors with congruent performance are necessary.[49–51] F$_4$BDOPV-2T and a high-mobility isoindigo polymer IIDDT-C3 were used as the n-channel and p-channel materials for the inverters, respectively (Figure 3f).[52] IIDDT-C3 exhibited hole mobilities of 1–1.5 cm^2 V^{-1} s^{-1} and on/off ratios of 10^4–10^5 using TGBC configuration. Owing to the high electron mobility and good stability of F$_4$BDOPV-2T under ambient conditions, polymeric complementary inverters with both n-type and p-type mobilities higher than 1 cm^2 V^{-1} s^{-1} are demonstrated for the first time. Figure 3g shows the static transfer characteristics of a complementary inverter at different voltages. Unlike those ambipolar polymeric inverters that cannot be switched off completely,[53,54] these complementary inverters displayed clearly on and off states and their V_{OUT} voltages were close to the V_{DD} supply voltage. The inverters demonstrated high gain values of up to 50 (Figure 3h). Our results imply that the semiconducting polymer-based devices could be used in complex logic circuits with high noise immunity and low static power consumption.

Grazing incident X-ray diffraction (GIXD) results indicated that F$_4$BDOPV-2T showed highly ordered edge-on packing with small π–π stacking distances of 3.52 Å (Table 2 and Figure S12, Supporting Information), which is probably the smallest π–π stacking distance in donor–acceptor-conjugated polymers,[30,55] largely due to the more planar backbone and stronger interchain interactions. To compare the film microstructures of two polymers, we calculated the polymer coherence length using the Scherrer's equation. The coherence lengths of F$_4$BDOPV-2T are estimated to be 15.5 nm and 8.1 nm for (200) and (010) diffractions, larger than those of F$_4$BDOPV-2Se (7.3 and 5.9 nm). The coherence length is related to both the degree of crystalline disorder and the number of scattering lattice plains in a crystallite.[56] Therefore, the lower mobility of F$_4$BDOPV-2Se could be explained by its relatively low molecular weight and less ordered molecular packing (see the Supporting Information).

Although a significant amount of FET devices based on F$_4$BDOPV-2T showed nonlinear transfer characteristics, we found that some of the FET devices based on F$_4$BDOPV-2T showed almost ideal transfer curves with good electron mobilities in the range of 1–2 cm^2 V^{-1} s^{-1} (**Figure 4**a). To understand the origin of this phenomenon, we fabricated FET devices
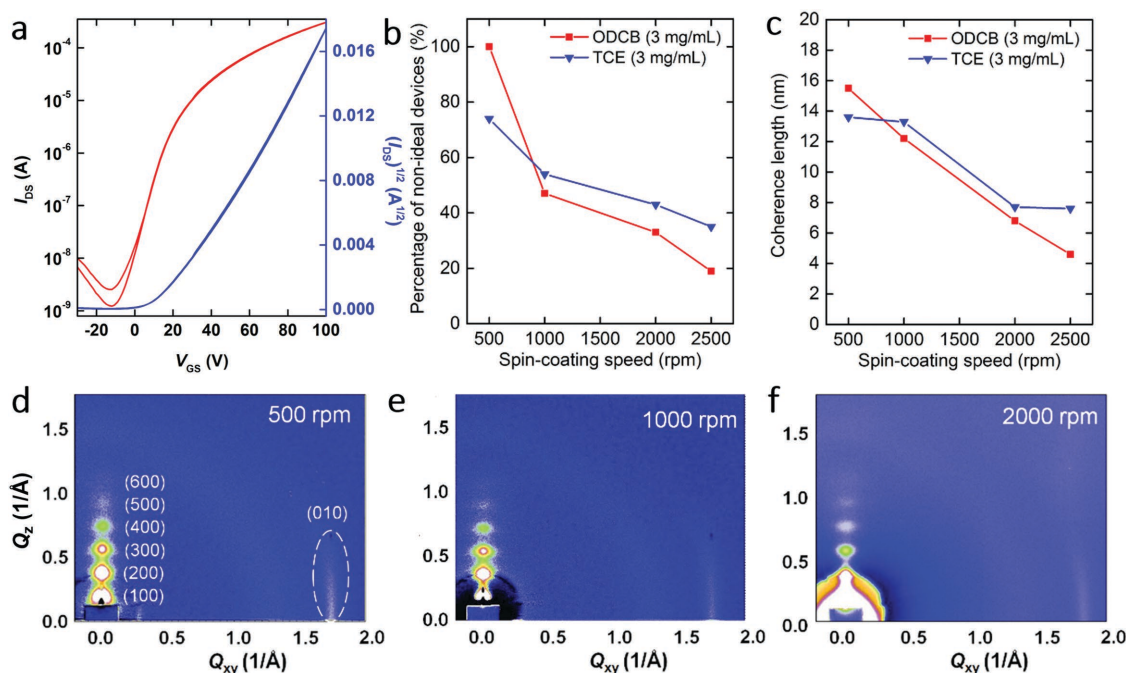
Figure 4. a) A near-ideal transfer characteristic observed in $F_4BDOPV-2T$ FET devices ($W = 2000$ um, $L = 100$ um, $V_{DS} = 100$ V). b) The percentage of nonlinear devices versus spin-coating speed using different solvents (over 20 devices were tested for each condition). c) Coherence length (L_c) variation versus spin-coating speed. The coherent lengths are calculated using the Scherrer equation based on the full width at half maximum of (200) diffraction peaks using GIXD data. 2D-GIXD patterns of $F_4BDOPV-2T$ films fabricated under different spin-coating speed (ODCB 3 mg mL^{-1}), d) 500 rpm, e) 1000 rpm, and f) 2000 rpm.

using two different solvents, o-dichlorobenzene (ODCB, b.p. 180 °C) and trichloroethylene (TCE, b.p. 87 °C) under different spin-coating speeds. As shown in Figure 4b, the percentage of the nonlinear devices decreased as increasing the spin-coating speed. When using ODCB as solvent and spin-coating at a low speed of 500 rpm, all the devices showed nonlinear transfer characteristics, whereas at a high speed of 2500 rpm, the percentage of nonlinear devices decreased to 19%. The mobilities also decreased as increasing the spin-coating speed (Figure S11, Supporting Information). To compare the film microstructures under different conditions, the polymer coherence lengths were calculated using the (200) diffractions from GIXD (Figure 4d–f). The devices fabricated at 500 rpm and using ODCB solution showed a large coherence length of 15.5 nm, which is comparable to the state-of-the-art p-type polymer transistors fabricated via slow-evaporation and alignment method.[9,19] Increasing the spin-coating speed to 2500 rpm, the coherence length of the polymer film decreased to 4.6 nm. Polymer films fabricated under low spin-coating speeds have clearly larger coherence lengths (Figure 4c). The increased coherence length in the lamellar stacking indicates larger crystallite domains and better polymer stacking order.[57] Thus, the nonlinear transfer characteristics highly correlates with film microstructures and the degree of crystalline order in polymer films. Using TCE as the solvent also showed similar trend that lower spin-coating speed and higher crystallinity films lead to higher percentage of nonlinear transfer curves. This confirms that the ODCB results are not artifacts and also not solvent related.

Although many suggestions have been made to explain the nonlinear transfer curves, such as contact resistance effect or the nonsaturated behavior in high V_G region,[31] yet our work clearly show that keeping polymer batch and dielectric layer the same, the transformation between near-ideal curves and nonlinear curves depends on different fabrication conditions without causing contact problem or nonsaturated behavior in output curves. Nguyen and co-workers proposed that the nonlinear transfer curves are attributed to the electron trapping of the SiO_2 dielectric layer.[32] However, we used defect-free CYTOP as the dielectric layer and still observed similar nonlinear transfer characteristics. Therefore, the nonlinear transfer curves cannot be simply explained by the dielectric trapping effect. Instead, we believe that this behavior is the intrinsic property of the semiconducting layer. Film morphology study showed that lower spin-coating speed leads to more ordered molecular packing and higher possibility of nonlinear transfer curves, whereas a high spin-coating speed will result in less-ordered molecular packing and near ideal transfer curves. However, further investigations are needed to understand the nonlinear transfer characteristics, but are beyond the scope of this work.

In summary, we have developed a strong electron-deficient building block F_4BDOPV with a deep LUMO level of -4.44 eV. The introduction of four fluorine atoms not only lowers the polymer LUMO levels, but also provides nonbonding interactions with the donor unit, thereby endowing polymers with planar backbones and locked conformations. All these features together provide $F_4BDOPV-2T$ with high electron mobilities and good device stability in air. Both polymers showed nonlinear transfer curves. We demonstrate that the nonlinear transfer curves can be changed to near-ideal transfer curves by tuning device fabrication conditions and propose that film

COMMUNICATION

morphology and microstructures may greatly contribute to the nonlinear transfer curves in polymer systems.

Experimental Section

Materials: Chemical reagents and CYTOP were purchased and used as received. All air- and water-sensitive reactions were performed under nitrogen atmosphere. Toluene and tetrahydrofuran (THF) were distilled from sodium prior to use. Branched alkyl chain, 19-(3-iodopropyl)heptatriacontane, is commercial available from Lyn (Beijing) Science & Technology Co., Ltd. Synthesis and characterization for all new compounds are detailed in Supplementary Information.

General Procedure for the Stille Polymerization: F$_4$BDOPV-2T:F$_4$BDOPV (60.0 mg, 0.0333 mmol), 5,5′-bis(trimethylstannyl)-2,2′-bithiophene (16.4 mg, 0.0333 mmol), Pd$_2$(dba)$_3$ (1.2 mg, 4 mol%), P(*o*-tol)$_3$ (1.6 mg, 16 mol%), and 15 mL of toluene were added to a Schlenk tube. The tube was charged with nitrogen through a freeze-pump-thaw cycle for three times. The mixture was stirred for 48 h at 110 °C. *N,N*′-diethylphenylazothioformamide (5 mg) was added and then the mixture was stirred for 1 h to remove any residual catalyst before being precipitated into methanol (200 mL). The precipitate was filtered through a nylon filter and purified via Soxhlet extraction for 8 h with acetone, 12 h with hexane, and finally collected with chloroform. The chloroform solution was then concentrated by evaporation and precipitated into methanol (200 mL) and filtered off to afford a dark solid (59 mg, yield 97%). M_n = 38.0 kDa, PDI: 2.74. Elemental Anal. Calcd: for (C$_{114}$H$_{170}$F$_4$N$_2$O$_6$S$_2$)$_n$: C, 75.83; H, 9.55; N, 1.55; Found: C, 77.19; H, 10.18; N, 1.57.

F$_4$BDOPV-2Se: The synthetic procedure is similar to that of F$_4$BDPPV-2T. (Yield: 82%). 23.8 kDa, PDI: 2.87. Elemental Anal. Calcd: for (C$_{114}$H$_{170}$F$_4$N$_2$O$_6$Se$_2$)$_n$: C, 72.12; H, 9.03; N, 1.48; Found: C, 70.73; H, 8.95; N, 1.22.

Device Fabrication and Characterization: Top-gate/bottom-contact FET devices and complementary inverters were fabricated using n^{++}-Si/SiO$_2$ (300 nm) or glass as substrates. The source and drain bottom electrodes (Ti (5 nm)/Au (40 nm)) were patterned by photolithography on substrate. The substrates were subjected to cleaning using ultrasonicator in acetone, cleaning agent, deionized water (twice), and isopropanol. The cleaned substrates were dried under vacuum at 80 °C and then transferred into a glovebox. A thin film of the polymer was deposited on the treated substrates by spin-coating at 500, 1000, 2000, and 2500 rpm for 60 s using a polymer solution (3 mg mL^{-1}), optionally followed by thermal annealing at 160 °C, 180 °C, 200 °C, 220 °C, 240 °C, and 260 °C for 10 min. In order to define n- and p-channel transistors on a complementary inverter, a substrate was partially covered by thin PDMS stamp during deposition of polymer films. After polymer film deposition, a CYTOP solution (CTL809M:CT-solv180 = 3:1) was spin-coated onto the semiconducting layer at 2000 rpm for 60 s resulting in a dielectric layer of 500 nm thick. The CYTOP layer was then baked at 100 °C for 1 h. Gate electrodes comprising a layer of Al (50 nm) were then evaporated through a shadow mask onto the dielectric layer by thermal evaporation.

The evaluations of the FETs and inverters were carried out in atmosphere (humidity 50%–60%) on a probe stage using a Keithley 4200 SCS as parameter analyzer. The carrier mobility, μ, was calculated from the data in the saturated regime according to the equation $I_{SD} = (W/2L)C_i\mu(V_G - V_T)^2$, where I_{SD} is the drain current in the saturated regime. W and L are the semiconductor channel width and length, respectively. C_i (3.7 nF for 500 nm CYTOP) is the capacitance per unit area of the gate dielectric layer, and V_G and V_T are the gate voltage and threshold voltage. $V_G - V_T$ of the device was determined from the relationship between the square root of I_{SD} and V_G at the saturated regime.

Supporting Information

Supporting Information is available from Wiley Online Library or from the author.

[1] Z. B. Henson, K. Müllen, G. C. Bazan, *Nat. Chem.* **2012**, *4*, 699.

[2] O. Knopfmacher, M. L. Hammock, A. L. Appleton, G. Schwartz, J. Mei, T. Lei, J. Pei, Z. Bao, *Nat. Commun.* **2014**, *5*, 2954.

[3] G. Schwartz, B. C.-K. Tee, J. Mei, A. L. Appleton, D. H. Kim, H. Wang, Z. Bao, *Nat. Commun.* **2013**, *4*, 1859.

[4] M. S. White, M. Kaltenbrunner, E. D. Głowacki, K. Gutnichenko, G. Kettlgruber, I. Graz, S. Aazou, C. Ulbricht, D. A. M. Egbe, M. C. Miron, Z. Major, M. C. Scharber, T. Sekitani, T. Someya, S. Bauer, N. S. Sariciftci, *Nat. Photonics* **2013**, *7*, 811.

[5] J. Mei, Y. Diao, A. L. Appleton, L. Fang, Z. Bao, *J. Am. Chem. Soc.* **2013**, *135*, 6724.

[6] J. Takeya, M. Yamagishi, Y. Tominari, R. Hirahara, Y. Nakazawa, T. Nishikawa, T. Kawase, T. Shimoda, S. Ogawa, *Appl. Phys. Lett.* **2007**, *90*, 102120.

[7] Y. Yuan, G. Giri, A. L. Ayzner, A. P. Zoombelt, S. C. B. Mannsfeld, J. Chen, D. Nordlund, M. F. Toney, J. Huang, Z. Bao, *Nat. Commun.* **2014**, *5*, 3005.

[8] I. Kang, H.-J. Yun, D. S. Chung, S.-K. Kwon, Y.-H. Kim, *J. Am. Chem. Soc.* **2013**, *135*, 14896.

[9] C. Luo, A. K. K. Kyaw, L. A. Perez, S. Patel, M. Wang, B. Grimm, G. C. Bazan, E. J. Kramer, A. J. Heeger, *Nano Lett.* **2014**, *14*, 2764.

[10] J.-H. Dou, Y.-Q. Zheng, Z.-F. Yao, T. Lei, X. Shen, X.-Y. Luo, Z.-A. Yu, S.-D. Zhang, G. Han, Z. Wang, Y. Yi, J.-Y. Wang, J. Pei, *Adv. Mater.* **2015**, *27*, 8051.

[11] F. Zhang, Y. Hu, T. Schuettfort, C. Di, X. Gao, C. R. McNeill, L. Thomsen, S. C. Mannsfeld, W. Yuan, H. Sirringhaus, D. Zhu, *J. Am. Chem. Soc.* **2013**, *135*, 2338.

[12] H.-J. Yun, S.-J. Kang, Y. Xu, S. O. Kim, Y.-H. Kim, Y.-Y. Noh, S.-K. Kwon, *Adv. Mater.* **2014**, *26*, 7300.

[13] T. Lei, X. Xia, J.-Y. Wang, C.-J. Liu, J. Pei, *J. Am. Chem. Soc.* **2014**, *136*, 2135.

[14] H. Klauk, U. Zschieschang, J. Pflaum, M. Halik, *Nature* **2007**, *445*, 745.

[15] J. Zaumseil, H. Sirringhaus, *Chem. Rev.* **2007**, *107*, 1296.

[16] X. Gao, Y. Hu, *J. Mater. Chem. C* **2014**, *2*, 3099.

[17] C. Wang, H. Dong, W. Hu, Y. Liu, D. Zhu, *Chem. Rev.* **2012**, *112*, 2208.

[18] Z. Yan, B. Sun, Y. Li, *Chem. Commun.* **2013**, *49*, 3790.

[19] H.-R. Tseng, H. Phan, C. Luo, M. Wang, L. A. Perez, S. N. Patel, L. Ying, E. J. Kramer, T.-Q. Nguyen, G. C. Bazan, A. J. Heeger, *Adv. Mater.* **2014**, *26*, 2993.

[20] B. H. Lee, B. B. Y. Hsu, S. N. Patel, J. Labram, C. Luo, G. C. Bazan, A. J. Heeger, *Nano Lett.* **2016**, *16*, 314.

[21] H.-R. Tseng, L. Ying, B. B. Y. Hsu, L. A. Perez, C. J. Takacs, G. C. Bazan, A. J. Heeger, *Nano Lett.* **2012**, *12*, 6353.

[22] J. Yao, C. Yu, Z. Liu, H. Luo, Y. Yang, G. Zhang, D. Zhang, *J. Am. Chem. Soc.* **2016**, *138*, 173.

[23] J. Lee, A.-R. Han, J. Kim, Y. Kim, J. H. Oh, C. Yang, *J. Am. Chem. Soc.* **2012**, *134*, 20713.

[24] J. Lee, A.-R. Han, H. Yu, T. J. Shin, C. Yang, J. H. Oh, *J. Am. Chem. Soc.* **2013**, *135*, 9540.

[25] H. Chen, Y. Guo, G. Yu, Y. Zhao, J. Zhang, D. Gao, H. Liu, Y. Liu, *Adv. Mater.* **2012**, *24*, 4618.

[26] I. Kang, T. K. An, J. Hong, H.-J. Yun, R. Kim, D. S. Chung, C. E. Park, Y.-H. Kim, S.-K. Kwon, *Adv. Mater.* **2013**, *25*, 524.

[27] J. Li, Y. Zhao, H. S. Tan, Y. Guo, C. Di, G. Yu, Y. Liu, M. Lin, S. H. Lim, Y. Zhou, H. Su, B. S. Ong, *Sci. Rep.* **2012**, *2*, 754.

[28] T. Lei, Y. Cao, Y. Fan, C.-J. Liu, S.-C. Yuan, J. Pei, *J. Am. Chem. Soc.* **2011**, *133*, 6099.

[29] T. Lei, J.-H. Dou, J. Pei, *Adv. Mater.* **2012**, *24*, 6457.

[30] J. Mei, D. H. Kim, A. L. Ayzner, M. F. Toney, Z. Bao, *J. Am. Chem. Soc.* **2011**, *133*, 20130.

[31] H. Sirringhaus, *Adv. Mater.* **2014**, *26*, 1319.

[32] H. Phan, M. Wang, G. C. Bazan, T.-Q. Nguyen, *Adv. Mater.* **2015**, *27*, 7004.

[33] J. D. Yuen, F. Wudl, *Energy Environ. Sci.* **2013**, *6*, 392.

[34] H. Usta, C. Risko, Z. Wang, H. Huang, M. K. Deliomeroglu, A. Zhukhovitskiy, A. Facchetti, T. J. Marks, *J. Am. Chem. Soc.* **2009**, *131*, 5586.

[35] X. Zhan, A. Facchetti, S. Barlow, T. J. Marks, M. A. Ratner, M. R. Wasielewski, S. R. Marder, *Adv. Mater.* **2011**, *23*, 268.

[36] J.-H. Dou, Y.-Q. Zheng, Z.-F. Yao, Z.-A. Yu, T. Lei, X. Shen, X.-Y. Luo, J. Sun, S.-D. Zhang, Y.-F. Ding, G. Han, Y. Yi, J.-Y. Wang, J. Pei, *J. Am. Chem. Soc.* **2015**, *137*, 15947.

[37] H. E. Katz, A. J. Lovinger, J. Johnson, C. Kloc, T. Siegrist, W. Li, Y.-Y. Lin, A. Dodabalapur, *Nature* **2000**, *404*, 478.

[38] P. Gawrys, D. Boudinet, M. Zagorska, D. Djurado, J.-M. Verilhac, G. Horowitz, J. Pécaud, S. Pouget, A. Pron, *Synth. Met.* **2009**, *159*, 1478.

[39] T. Lei, J.-H. Dou, X.-Y. Cao, J.-Y. Wang, J. Pei, *J. Am. Chem. Soc.* **2013**, *135*, 12168.

[40] T. Lei, J.-H. Dou, X.-Y. Cao, J.-Y. Wang, J. Pei, *Adv. Mater.* **2013**, *25*, 6589.

[41] R. S. Rowland, R. Taylor, *J. Phys. Chem.* **1996**, *100*, 7384.

[42] N. E. Jackson, B. M. Savoie, K. L. Kohlstedt, M. Olvera de la Cruz, G. C. Schatz, L. X. Chen, M. A. Ratner, *J. Am. Chem. Soc.* **2013**, *135*, 10475.

[43] P. Prins, F. C. Grozema, J. M. Schins, S. Patil, U. Scherf, L. D. Siebbeles, *Phys. Rev. Lett.* **2006**, *96*, 146601.

[44] Y.-Q. Zheng, Z. Wang, J.-H. Dou, S.-D. Zhang, X.-Y. Luo, Z.-F. Yao, J.-Y. Wang, J. Pei, *Macromolecules* **2015**, *48*, 5570.

[45] J. Kim, T. M. Swager, *Nature* **2001**, *411*, 1030.

[46] R. Steyrleuthner, M. Schubert, I. Howard, B. Klaumunzer, K. Schilling, Z. Chen, P. Saalfrank, F. Laquai, A. Facchetti, D. Neher, *J. Am. Chem. Soc.* **2012**, *134*, 18303.

[47] C. Zhang, Y. Zang, E. Gann, C. R. McNeill, X. Zhu, C. A. Di, D. Zhu, *J. Am. Chem. Soc.* **2014**, *136*, 16176.

[48] T. He, M. Stolte, F. Würthner, *Adv. Mater.* **2013**, *25*, 6951.

[49] S.-M. Kang, Y. Leblebici, *Cmos Digital Integrated Circuits: Analysis and Design*, 3rd ed., McGraw-Hill, **2003**, New York, USA.

[50] K. Kawabata, I. Osaka, M. Nakano, N. Takemura, T. Koganezawa, K. Takimiya, *Adv. Electron. Mater.* **2015**, *1*, 1500039.

[51] H. Chen, Y. Guo, Z. Mao, G. Yu, J. Huang, Y. Zhao, Y. Liu, *Chem. Mater.* **2013**, *25*, 3589.

[52] T. Lei, J.-H. Dou, J. Pei, *Adv. Mater.* **2012**, *24*, 6457.

[53] A. J. Kronemeijer, E. Gili, M. Shahid, J. Rivnay, A. Salleo, M. Heeney, H. Sirringhaus, *Adv. Mater.* **2012**, *24*, 1558.

[54] T. Lei, J.-H. Dou, Z.-J. Ma, C.-J. Liu, J.-Y. Wang, J. Pei, *Chem. Sci.* **2013**, *4*, 2447.

[55] X. Zhang, H. Bronstein, A. J. Kronemeijer, J. Smith, Y. Kim, R. J. Kline, L. J. Richter, T. D. Anthopoulos, H. Sirringhaus, K. Song, M. Heeney, W. Zhang, I. McCulloch, D. M. DeLongchamp, *Nat. Commun.* **2013**, *4*, 2238.

[56] J. Rivnay, S. C. B. Mannsfeld, C. E. Miller, A. Salleo, M. F. Toney, *Chem. Rev.* **2012**, *112*, 5488.

[57] J. Rivnay, R. Noriega, J. E. Northrup, R. J. Kline, M. F. Toney, A. Salleo, *Phys. Rev. B* **2011**, *83*, 121306.

[58] H. Bronstein, J. M. Frost, A. Hadipour, Y. Kim, C. B. Nielsen, R. S. Ashraf, B. P. Rand, S. Watkins, I. McCulloch, *Chem. Mater.* **2013**, *25*, 277.

[59] I. Osaka, T. Abe, S. Shinamura, K. Takimiya, *J. Am. Chem. Soc.* **2011**, *133*, 6852.